Visualization and simulation of physical phenomena in the aircraft icing process

Ivan A. Amelyushkin

Department of aerothermodynamics of flying vehicles, Central aerohydrodynamic institute (TsAGI), Zhukovsky, Moscow region, Russia
Amelyushkin_Ivan@mail.ru

Abstract The process of ice accretion is under investigation. Original algorithms were proposed in order to determine two phase flow parameters via laser sheet images analysis. A numerical algorithm was developed in order to calculate carrying gas parameters fields (velocity, pressure, etc.) via processing particulate velocity fields. Differences of particle velocity and carrying gas velocity were taken in account. A criterion of two phase velocity nonequilibrium was proposed. Aerosol flows with nonspherical ice crystals were also investigated. An optical system and numerical algorithms of image processing were developed in order to visualize two phase flow and to determine particle and droplet concentration (mass, volumetric and numerical) as well as size distribution near a solid body in the aerosol flow. The parallel-sided laser sheet was used in order to simplify image processing and apply methods of inverse problems' solution in image analysis. These methods were developed to take into account several physical effects. Mathematical models of supercooled water droplets stability and their crystallization were proposed and developed. Minimal values of the supercooled droplets impingement speed were measured in order to determine flow parameters when droplets stay liquid ones after collisions with the aircraft surface. Original mathematical models of stochastic motion of nonspherical ice crystals and small water droplets were developed.
Keywords: laser sheet, two phase flow diagnostics, inverse problems, supercooled droplets, crystallization front, nonspherical particles

1 Introduction

The goal of a present work is to increase information value of nonintrusive two-phase flow investigation via laser sheet image analysis and to develop mathematical models of physical processes in aircraft icing process. For instance a use of traditional methods of measuring gas velocities via particles' images analysis can be problematic due to significant differences between particles' velocities and carrying flow velocity. These differences can take place in supersonic high gradient and low density flows[1, 2] and also in flows with massive particles (in particular wind tunnel aircraft icing investigation [3, 4]). Precision particles' concentration measurement via laser sheet image analysis [1, 5] could be increased via improving laser sheet optics and developing methods of inverse problems' solution. The process of the ice accretion on a body surface is being under investigation almost during the whole aviation history, but up today the physics of this process needs more deep understanding. It concerns especially an initial touch of a supercooled drop to a solid body surface. Supercoolled water droplet crystallization after impingement and its adhesion (to an aircraft surface) mechanisms are fundamental problems in mechanics of the multiphase flows as well as in a condensed-matter physics.

2 Gas parameters reconstruction via particle velocity field processing

The simplest way of gas velocity field (which may significantly differ from particles velocity field) correction could be connected with well-known Stokes's Cd – drag coefficient model (Cd = 24/Re) which could be applied for small differences between particle and gas velocities, and as result small Reynolds numbers $\mathrm{Re}=2a_p|\boldsymbol{V}-\boldsymbol{V_p}|/\mu$ both for stationary and non-stationary flows. Here $\boldsymbol{V}$ and $\boldsymbol{V_p}$ – velocity vectors of gas and particles, ρ_p and a_p – particle's material density and its average radius, μ – dynamic gas viscosity. In this case because of small influence of temperature on particle motion in the gas in most practical tasks there is no need to calculate density field and the correction procedure may be expressed by the following equation: $\boldsymbol{V}=\boldsymbol{V_p}+\left[\frac{\partial \boldsymbol{V}_p}{\partial t}+(\boldsymbol{V}_p\cdot\bar{\nabla})\boldsymbol{V}_p\right]\frac{2\rho_p a_p^2}{9\mu(T)}$,

Pressure gradient could be obtained from the flowing equation: $\nabla P=\rho\left(\frac{\partial \boldsymbol{V}}{\partial t}+(\boldsymbol{V}\cdot\bar{\nabla})\boldsymbol{V}\right)+\nabla\mathbf{T}(\mu(T),\boldsymbol{V})+\rho\boldsymbol{g}$

Here $\mathbf{T} = \mu(T)\begin{pmatrix} 2\frac{\partial u}{\partial x} & \frac{\partial u}{\partial y}+\frac{\partial v}{\partial x} & \frac{\partial u}{\partial z}+\frac{\partial w}{\partial x} \\ \frac{\partial v}{\partial x}+\frac{\partial u}{\partial y} & 2\frac{\partial v}{\partial y} & \frac{\partial v}{\partial z}+\frac{\partial w}{\partial y} \\ \frac{\partial w}{\partial x}+\frac{\partial u}{\partial z} & \frac{\partial w}{\partial y}+\frac{\partial v}{\partial z} & 2\frac{\partial w}{\partial z} \end{pmatrix}$ – is a stress tensor, $\boldsymbol{g}$ is a free fall acceleration vector. For incompressible flows algorithms of pressure reconstruction via velocity of particles field analysis were developed in [6] image. In case of stationary flow in order to obtaine self-contained system let us write energy balance equation: $\nabla(E \cdot \boldsymbol{V}) = \mu\Psi$.

Here $E = \rho\frac{u^2+v^2+w^2}{2} + \frac{\gamma}{\gamma-1}P$, $\Psi = \frac{\partial}{\partial x}\left(u\tau_{xx} + v\tau_{xy} + w\tau_{xz}\right) + \frac{\partial}{\partial y}\left(u\tau_{xy} + v\tau_{yy} + w\tau_{yz}\right) + \frac{\partial}{\partial z}\left(u\tau_{zx} + v\tau_{zy} + w\tau_{zz}\right) =$

$$= \frac{\partial}{\partial x}\left(2u\frac{\partial u}{\partial x} + v\left(\frac{\partial u}{\partial y}+\frac{\partial v}{\partial x}\right) + w\left(\frac{\partial w}{\partial x}+\frac{\partial u}{\partial z}\right)\right) + \frac{\partial}{\partial y}\left(u\left(\frac{\partial u}{\partial y}+\frac{\partial v}{\partial x}\right) + 2v\frac{\partial v}{\partial y} + w\left(\frac{\partial w}{\partial y}+\frac{\partial v}{\partial z}\right)\right) + \frac{\partial}{\partial z}\left(u\left(\frac{\partial w}{\partial x}+\frac{\partial u}{\partial z}\right) + v\left(\frac{\partial w}{\partial y}+\frac{\partial v}{\partial z}\right) + 2w\frac{\partial w}{\partial z}\right)$$

Taking into account expressions for pressure gradients and making use of ideal gas equation of state the last expression will be the following:

$$\frac{1}{3}\left[\frac{\partial u^3}{\partial x}+\frac{\partial v^3}{\partial y}+\frac{\partial w^3}{\partial z}\right] + uv\left(\frac{\partial v}{\partial x}+\frac{\partial u}{\partial y}\right) + uw\left(\frac{\partial w}{\partial x}+\frac{\partial u}{\partial z}\right) + vw\left(\frac{\partial w}{\partial y}+\frac{\partial v}{\partial z}\right) + \frac{P}{\rho}\frac{1}{2}\left(\frac{\partial u}{\partial x}+\frac{\partial v}{\partial y}+\frac{\partial w}{\partial z}\right) = \eta\left(\frac{\gamma-1}{2\gamma}\right)\Theta + \frac{\Xi}{2\gamma}$$

Here $\frac{\mu}{\rho}\Psi = \eta\Theta$, $\Xi = u\frac{\partial}{\partial x}\left(\frac{u^2+v^2+w^2}{2}\right) + v\frac{\partial}{\partial y}\left(\frac{u^2+v^2+w^2}{2}\right) + w\frac{\partial}{\partial z}\left(\frac{u^2+v^2+w^2}{2}\right)$.

$\eta = \eta(T)$ – kinematic gas viscosity, which depends on its temperature. The energy balance equation could be rewritten as follows: $\Phi + \frac{P}{\rho}\xi = \eta k + b$, where $\xi = \frac{1}{2}\left(\frac{\partial u}{\partial x}+\frac{\partial v}{\partial y}+\frac{\partial w}{\partial z}\right)$, $b = \frac{\Xi}{2\gamma}$, $k = \left(\frac{\gamma-1}{2\gamma}\right)\Theta$ and

$$\Phi = \frac{1}{3}\left[\frac{\partial u^3}{\partial x}+\frac{\partial v^3}{\partial y}+\frac{\partial w^3}{\partial z}\right] + uv\left(\frac{\partial v}{\partial x}+\frac{\partial u}{\partial y}\right) + uw\left(\frac{\partial w}{\partial x}+\frac{\partial u}{\partial z}\right) + vw\left(\frac{\partial w}{\partial y}+\frac{\partial v}{\partial z}\right).$$

Making use of ideal gas equation the equation of temperature will be the following one: $T\frac{R\xi}{\mu_0 k} - \eta(T) = \frac{b-\Phi}{k}$.

Or $T \cdot f(\boldsymbol{V}) - \eta(T) = g(\boldsymbol{V})$ – equation, in which f and g – functions which depend only on flow velocities, μ0 – gas molecular mass. It should be noted that neglecting viscous effects (not only because of low accuracy of second velocities' derivatives calculations, but also because of their small contribution to the flow behavior far away from the wall) equation for temperature determination depends linearly on temperature T: temperature is expressed in terms of first velocities derivatives. In case of steady flow neglecting viscid effects the expression for temperature will be the following:

$$T = -\frac{(2\gamma-3)\left(u^2\frac{\partial u}{\partial x} + v^2\frac{\partial v}{\partial y} + w^2\frac{\partial w}{\partial z}\right) + 3(2\gamma-1)\left[uv\left(\frac{\partial v}{\partial x}+\frac{\partial u}{\partial y}\right) + uw\left(\frac{\partial w}{\partial x}+\frac{\partial u}{\partial z}\right) + vw\left(\frac{\partial w}{\partial y}+\frac{\partial v}{\partial z}\right)\right]}{\left(\frac{\partial u}{\partial x}+\frac{\partial v}{\partial y}+\frac{\partial w}{\partial z}\right)}\frac{\mu}{3\gamma R}$$

In order to make a correction for velocity nonequilibrium two phase flow a Stokes drag coefficient model leads to significant mistakes. However Stokes drag coefficient model couldn't be applied correctly for big Reynolds numbers of flow around a particle, e.g. for high velocity gradient and low density flows[1, 2, 7], e.g. supersonic flows in shock wind tunnel (Fig. 1) and for flows with massive droplets or particles, e.g. in icing wind tunnel[3, 4]. In this case a use of more complex models (e.g. [8]) will lead to calculate gas density as it is in a particle motion equation and temperature as it changes significantly and as result influences on the viscosity which influences on particle motion.

In present work an original algorithm was developed to recover gas parameter via particle velocity field analysis whose velocities differ from carrying gas velocities. The algorithm was tested on several experimental examples and stability of inverse problem solution was proved (Fig 2, Fig. 3). A calculation of gas density, temperature and pressure requires involvement of equation of mass, pulse and energy conservation which as was mentioned above assumed to be perfect. Seven assumptions were made in order to solve inverse problem of gas parameters determination via particles motion analysis: 1. Particles' velocity field is known; 2. All particles are spherical and their radius is known and does not change; 3. A flow is

stationary; 4. Carrying fluid shearing stress is proportional to a rate of shearing strain, gas motion is expressed in terms of Navie-Stokes equations, dynamic viscosity coefficient of a gas depends only on temperature and expressed in terms of Sutherland's formula, gas is proposed to be perfect. Far way from a circumfluent body velocities of particles equals gas velocities, gas parameters (velocity, pressure and temperature) are known; 5. Particle's motion is described in terms of Basset-Boussinesq-Oseen equation; 6. Particle drag coefficient is models are taken from [2, 7]; 7. Presence of particles and their motion in a flow does not influence on a flow itself. With the assumption that a flow is one dimensional along the perpendicular to the shock wave front [7] (Fig. 1) equations of mass and energy concervation will be as follows: $\rho u = \rho_0 u_0 = \mathrm{Const}_m$; $u\left(\frac{\rho u^2}{2} + \frac{P\gamma}{\gamma - 1}\right) - u\mu_m(T)\frac{\partial u}{\partial x} = u_0\left(\frac{\rho_0 u_0^2}{2} + \frac{P_0\gamma}{\gamma - 1}\right) = \mathrm{Const}_E$.

It should be noted that as calculations shows a flow velocity tends to be equal particle velocity with taking smaller particles' radius for PIV images analysis.

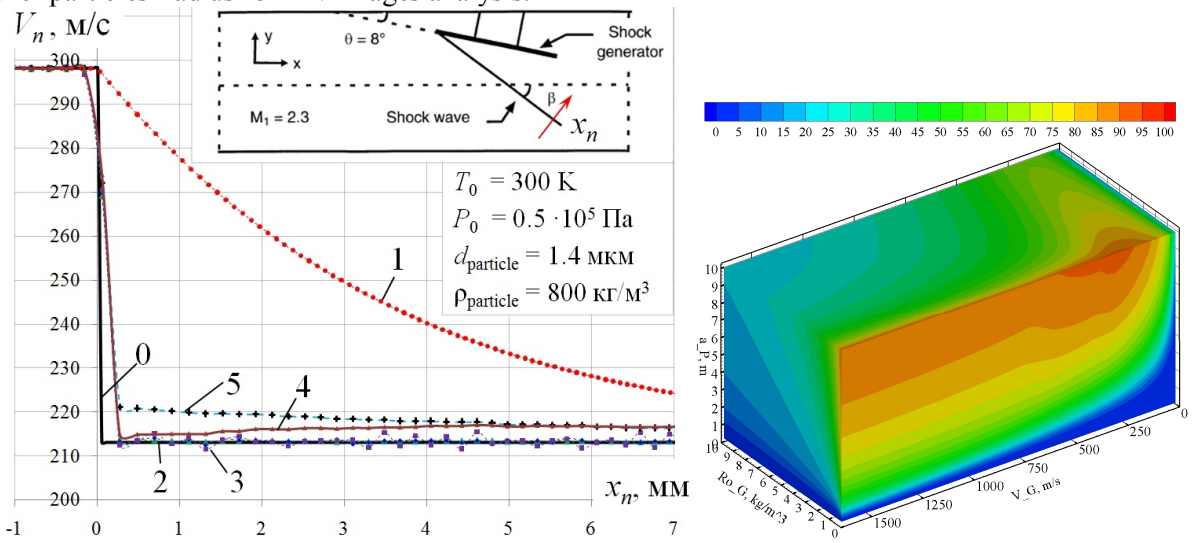

Fig. 1: On the left: example of gas velocity field determination via particles' velocity field and a scheme of experiment [2], 0 – exact value of gas velocity, 1 – velocity of particles, 2÷5 gas velocity field which was obtained via particle velocity field analysis at different values of mistakes in determination of particles' properties. On the right: two phase flow velocity nonequilibrium region in a space of its parameters: carrying particles gas velocity, particles material density and particle's radius.

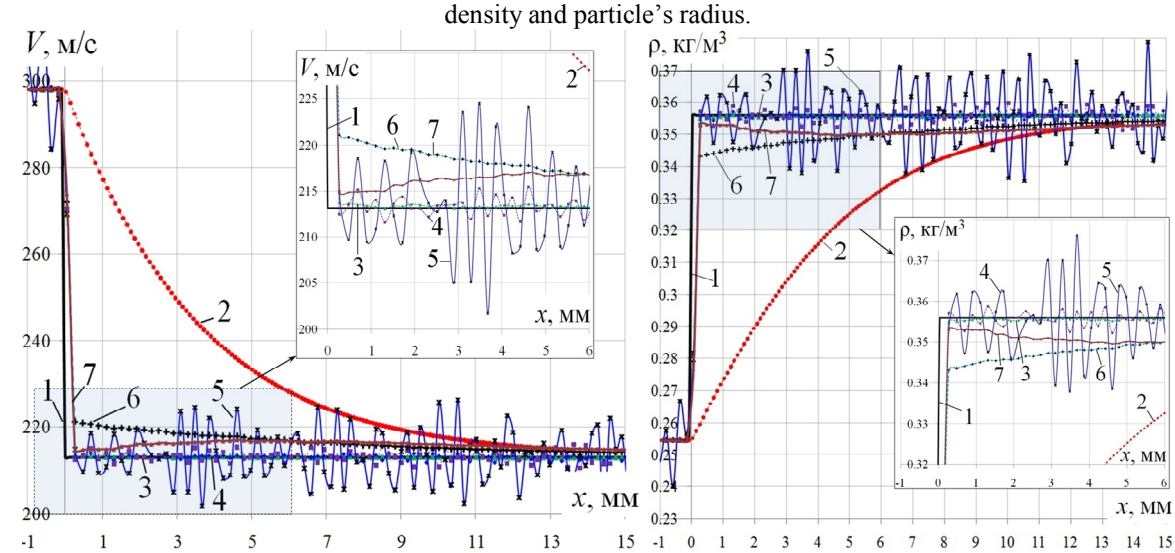

Fig. 2: Restoration of gas velocity (left) and density (right) via particle image velocity field: 1 – exact value of gas velocity (density) , 2 – velocity of particles, (density field which is based on particle's velocities), 2÷7 gas velocity (density at the right) field which was obtained via particle velocity field analysis at different values of mistakes in determination of properties of particles.

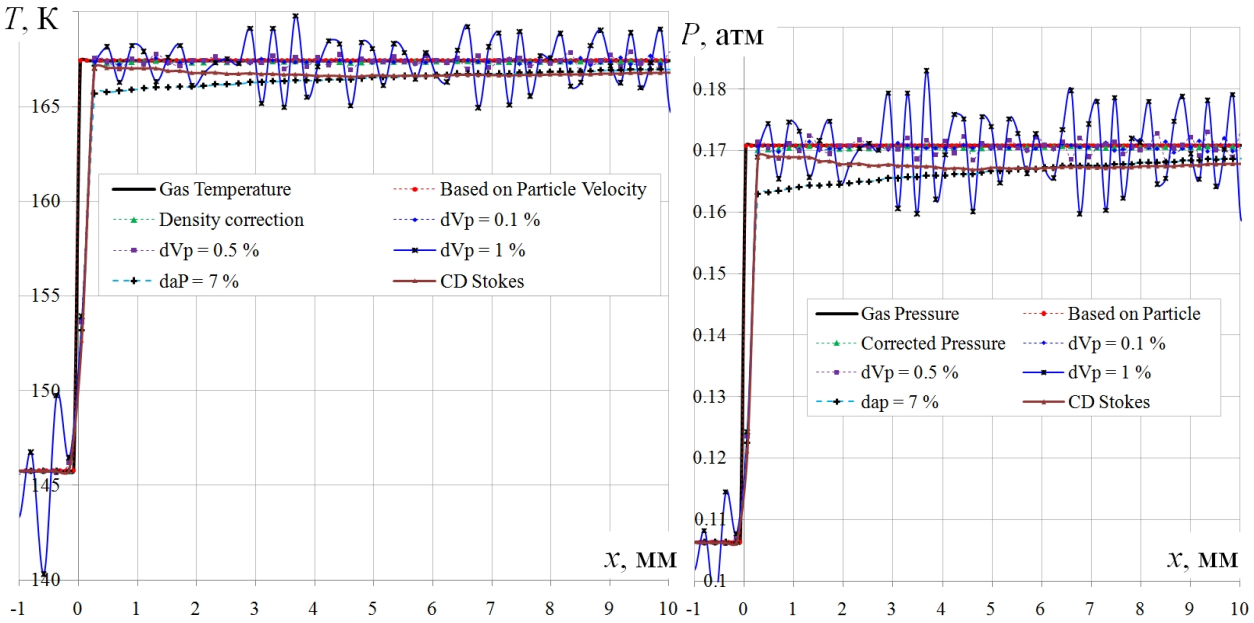

Fig. 3: Restoration of temperature (left) and pressure (right) fields via particle velocity field processing.

3 Diagnostics of two phase flow on a velocity nonequilibrium regions

One of the most common used disperse flows velocity criteria is a Stokes number which characterizes the flow in whole. In [9, 10] papers different two-phase flow velocity nonequilibrium criteria reviews are given in order to determine conditions under which particles velocimetry methods of flow diagnostics could be applied. An example of such conditions determination one can see in Fig. 4. However event at low values of Stokes numbers and other two phase flow velocity nonequilibrium criteria some regions of significant differences between particles' and gas velocities in a flow may take place. The goal of present paragraph is to determine regions with a given gas and particles velecities difference. Motion particle is described in terms of Basset-Bussinesque-Ozeen equation:

$$m_p \frac{\mathrm{d}\boldsymbol{V}_p}{\mathrm{d}t} = \frac{1}{2} C_D \pi a_p^2 \rho |\boldsymbol{V} - \boldsymbol{V}_p| (\boldsymbol{V} - \boldsymbol{V}_p) + \frac{4}{3}\pi a_p^3 \rho \frac{\mathrm{d}\boldsymbol{V}}{\mathrm{d}t} + \frac{2}{3}\pi a_p^3 \rho \frac{\mathrm{d}(\boldsymbol{V} - \boldsymbol{V}_p)}{\mathrm{d}t} + 6a_p^2 \sqrt{\pi \rho \mu} \int_{-\infty}^{t} \frac{1}{\sqrt{t-\tau}} \frac{\mathrm{d}(\boldsymbol{V} - \boldsymbol{V}_p)}{\mathrm{d}\tau} \mathrm{d}\tau + \sum \boldsymbol{F}$$

Here m_p – mass of the particle, a_p – radius of the particle, ρ – flow density, μ – dynamic viscosity of the flow, $\boldsymbol{V}$ – flow velocity, $\boldsymbol{V_p}$ – particle's velocity, t – time, C_D – particle's drag coefficient, which depends on its circumfluent regime. The first part in the right part of the equation corresponds to the aerohydrodynamic drag force, the second one is a gas acceleration force. The acceleration of the fluid leads to a pressure gradient in the vicinity of the particle and hence to the additional force given by the third term. The forth term is the 'Basset history integral's which defines the resistance caused by the unsteadiness of the flow. $\Sigma \boldsymbol{F}$ – are other forces, which also can act on a particle: e.g. Saffman force, electrostatic force, etc. The last equation can be simplified for gas flow, where its density is three times lower then density of particles' material. Neglecting $\Sigma \boldsymbol{F}$ the equation will be the following: $m_p \frac{\mathrm{d}\boldsymbol{V}_p}{\mathrm{d}t} = \frac{1}{2} C_D \pi a_p^2 \rho |\boldsymbol{V} - \boldsymbol{V_p}| \cdot (\boldsymbol{V} - \boldsymbol{V_p})$. Taking into account, that $\frac{\mathrm{d}}{\mathrm{d}t} = \frac{\partial}{\partial t} + (\boldsymbol{V}_p \cdot \bar{\nabla})$ and obtaining mass of the spherical particle from its density ρ_p and radius a_p, let us rewrite particles' motion equation:

$$\frac{\mathrm{d}\boldsymbol{V}_p}{\mathrm{d}t} = \frac{\partial \boldsymbol{V}_p}{\partial t} + (\boldsymbol{V}_p \cdot \bar{\nabla})\boldsymbol{V}_p = \frac{3}{8} C_D \frac{\rho}{\rho_p} \frac{1}{a_p} |\boldsymbol{V} - \boldsymbol{V_p}| \cdot (\boldsymbol{V} - \boldsymbol{V_p});$$

Let us designate $\boldsymbol{V} - \boldsymbol{V_p} = \boldsymbol{V}*$; Then $\frac{\mathrm{d}\boldsymbol{V}_p}{\mathrm{d}t} = ((\boldsymbol{V} - \boldsymbol{V}*) \cdot \bar{\nabla})(\boldsymbol{V} - \boldsymbol{V}*) = \frac{3}{8} C_D \frac{\rho}{\rho_p} \frac{1}{a_p} |\boldsymbol{V}*| \boldsymbol{V}*;$

Let us designate velocity components $\boldsymbol{V}*$ as follows $V_i^* = \alpha_i V_i$; here $i = \overline{1,3}$ $i.$ $|\boldsymbol{V}*| = \sqrt{\sum_{i=1}^{3} [V_i(1-\alpha_i)]^2}$, having experimental data of particles' velocity field in a two-phase flow, the system of equations will be following:

$$\frac{\partial V_p^i}{\partial t}+u_p\frac{\partial V_p^i}{\partial x}+v_p\frac{\partial V_p^i}{\partial y}+w_p\frac{\partial V_p^i}{\partial z}=\frac{9}{2}\frac{\mu}{\rho_p a_p^2}\frac{C_D}{C_D^{\mathrm{Stk}}}\left(V_i-V_p^i\right)=\frac{9}{2}\frac{\mu}{\rho_p a_p^2}\frac{C_D}{C_D^{\mathrm{Stk}}}\alpha_i V_i=\frac{9}{2}\frac{\mu}{\rho_p a_p^2}\xi\frac{\alpha_i}{1-\alpha_i}V_p^i,$$

$$\text{or}\quad A_i=\frac{\frac{\partial V_p^i}{\partial t}+u_p\frac{\partial V_p^i}{\partial x}+v_p\frac{\partial V_p^i}{\partial y}+w_p\frac{\partial V_p^i}{\partial z}}{\frac{9}{2}\frac{\mu}{\rho_p a_p^2}V_p^i}=A_i\left(u_p,v_p,w_p,\frac{9}{2}\frac{\mu}{\rho_p a_p^2}\right)=\xi\left(\alpha_x,\alpha_y,\alpha_z,\rho\right)\frac{\alpha_i}{1-\alpha_i}$$

Expressing one coefficient of two phase flow velocity nonequilibrium α_i from another two ones, we will obtain for each of three coefficients nonliniar algebraic equation, which can be solved if a flow density is known or in a case of incompressible flow: $A_i=\xi(\alpha_i,\rho)\frac{\alpha_i}{1-\alpha_i}$; $\alpha_j=\frac{A_j}{A_j+A_i(1-\alpha_i)/\alpha_i}$. In particular, in case of Stokes model of drag force, which acts on a particle we will obtain the following equation for coefficients α_i: $\alpha_i=\frac{A_i}{1+A_i}$. For two phase flow velocity equilibrium we will require $\alpha=\sqrt{\sum_{i=1}^{3}\alpha_i^2}<<1$. Let us define α as a criterion of two-phase flow velocity nonequilibrium, which may be used to characterize geometric places in disperse flow with a given velocity difference of phases.

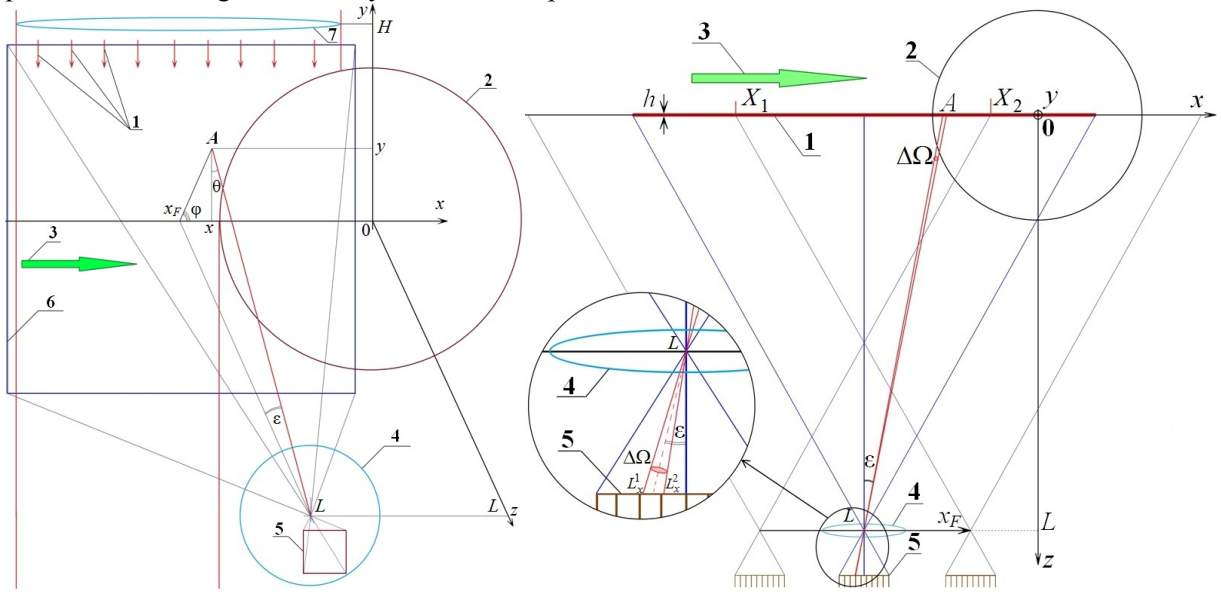

Fig. 5: On the left: scheme of laser sheet two phase flow diagnostics near a spherical body; on the right scheme of laser sheet polydisperse flow diagnostics near a spherical body and making images at different angles. 1 – laser sheet plane, 2– circumfluent body, 3 – two phase flow direction, 4– lens of photoreceiver, – image sensor.

4 Disperse phase parameters reconstruction via laser sheet image processing

In present work algorithm of particle concentration was developed for polydisperse two-phase flow and tested on several examples. An original method was developed in order to determine special particulate concentration (volumetric, numeric and mass concentration) size distribution in a polydisperse two-phase flow. A flow is lighted by monochromatic radiation plane (laser sheet). A description of laser sheet optics for parallel laser sheet construction is described in [11]. Two-phase flow parameters are determined via images processing. These image are obtained from different directions. While processing the following assumptions are made:

1. Particles (or droplets) have spherical shape and particles' material is also known. Their physical properties are well-known and does not depend on their sizes.
2. Monochromatic light absorption and scattering is described via well-known Mie theory. When particles' shapes are non-spherical, another experimental and theoretical approaches could be used;
3. Multiple scattering (reradiation) is proposed to be negligible due to the small light free path length because of the small particulate concentration. Light extinction is described in terms of Buger-Lambert-Beer's law:

$$\mathrm{d}I_\lambda = n_p Q_{\mathrm{Ext}}(a_p,\lambda)\pi a_p^2 I_\lambda \mathrm{d}x;$$

4. Light scattering on particles is coherent, light wavelength is known a priory.

Intensity of light $I_A^i(x,y)$ in each point $A(x, y)$ of the laser sheet plane $z = 0$ (Fig. 5) is proportional to the particulate concentration $n(x, y, 0)$ in a small vicinity of this point, laser sheet thickness h, and also light scattering coefficient $Q_\lambda^{\mathrm{Sca}}(a_p,\theta)$ of particle with a given radius a_p for a given wave laser length λ in θ direction (Fig. 5). In each point of space scattered light intensity in direction θ may be calculated from the following equation:

$$I_i(\theta) = n_i Q_\lambda^{\mathrm{Sca}}(a_p^i,\theta)\pi(a_p^i)^2 hI_0 = \frac{\rho_i}{\rho_p \frac{4}{3}\pi(a_p^i)^3} Q_\lambda^{\mathrm{Sca}}(a_i,\theta)\pi a_i^2 hI_0 = \frac{3\rho_i h}{\rho_p 4a_p^i} Q_\lambda^{\mathrm{Sca}}(a_p^i,\theta)I_0;$$

Here n_i and ρ_i – numeric and mass particles' concentration of i-th particles correspondently, ρ_p – particles' material density. The intensity of scattered light in θ direction could be obtained from the following system of j equations: $I(\theta) = \sum_{i=1}^{i_{\max}} I_i(\theta) = \frac{3hI_0}{4\rho_p}\sum_{i=1}^{i_{\max}} \frac{\rho_i}{a_p^i} Q_\lambda^{\mathrm{Sca}}(a_p^i,\theta)$, or $\sum_{i=1}^{i_{\max}} \frac{\rho_i}{a_p^i} Q_\lambda^{\mathrm{Sca}}(a_p^i,\theta_j) = \frac{4\rho_p}{3hI_0} I_j(\theta_j);$

The last expression is a system of linear j equations which could be solved via well-known Gaussian method. Thus a problem polidisperse flow mass concentration particles' size distribution field determination could be solved via making images at different angles and processing of obtained images according to described above algorithm.

$$I(y,\theta) = \frac{3h}{4\rho_p} I_0(y)\sum_{i=1}^{i_{\max}} \frac{\rho_i}{a_p^i} Q_\lambda^{\mathrm{Sca}}(a_p^i,\theta)\cdot$$

Intensity of light in each point y of the laser sheet plane is diminished due to light scattering and absorption by particles on a way from the source of light H. to the point y (Fig. 5). As a particle concentration is not too large for a necessity of taking into account light reradiation effects in present work a Beer-Lambert-Bouguer law of light extinction during its propagation through a flow with particles is used. The expression for intensity of light $I_0(y)$ in a point of laser sheet plane with coordinate y is the following:

$$I_0(y) = I_0 \cdot \exp\left[-\frac{3}{4\rho_p}\int_y^H \left(\sum_{i=1}^{i_{\max}} \frac{\rho_i(y)}{a_p^i} Q_\lambda^{\mathrm{Sca}}(a_p^i,\theta)\right)\mathrm{d}y'\right];$$

Thus intensity of radiation which is scattered by particles in direction of angle θ (Fig. 5, Fig. 6) is the following:

$$I(y,\theta) = \frac{3h}{4\rho_p} I_0 \exp\left[-\frac{3}{4\rho_p}\int_y^H \left(\sum_{i=1}^{i_{\max}} \frac{\rho_i(y)}{a_p^i} Q_\lambda^{\mathrm{Ext}}(a_p^i)\right)\mathrm{d}y'\right]\cdot\sum_{i=1}^{i_{\max}} \frac{\rho_i}{a_p^i} Q_\lambda^{\mathrm{Sca}}(a_p^i,\theta);$$

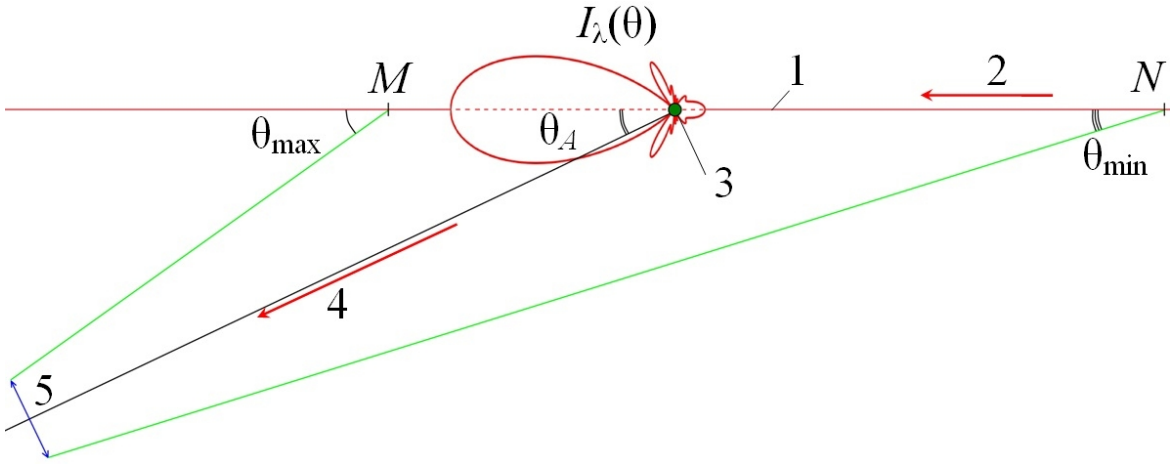

Fig. 6: scheme of image registration under angle: 1 – laser sheet plane, 2 – light propagation direction, 3 – scattering centre, 4 – scattered light direction, 5 – photoreceiver.

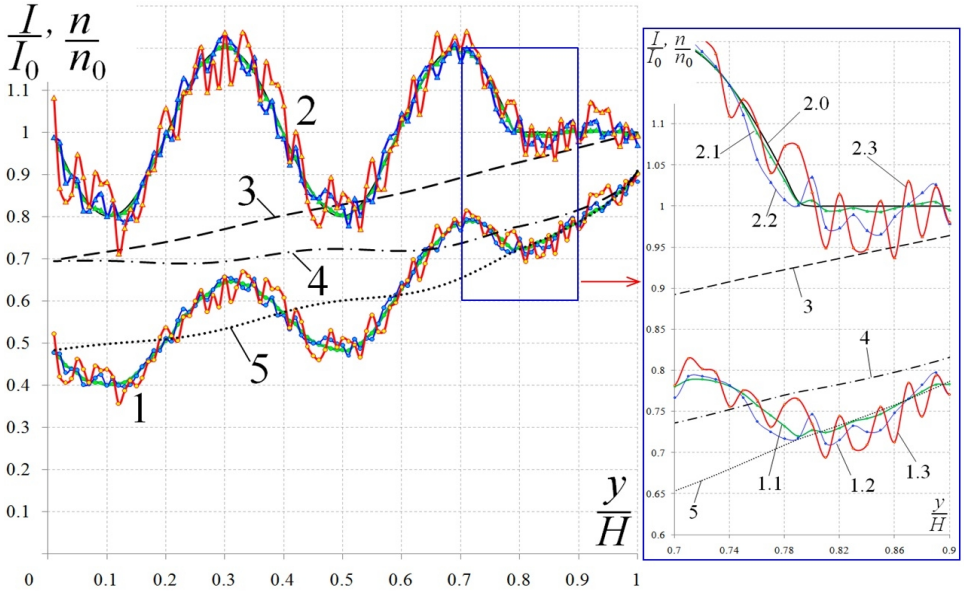

Fig. 7: Example of investigation of stability of inverse problem solution, x = const: 1 – intensity of light on laser sheet image, 2 – monodisperse particles' numeric concentration distribution, 3, 4 and 5 – light extinction in a laser sheet plane, on a way from a plane to photoreceiver and total correspondingly.

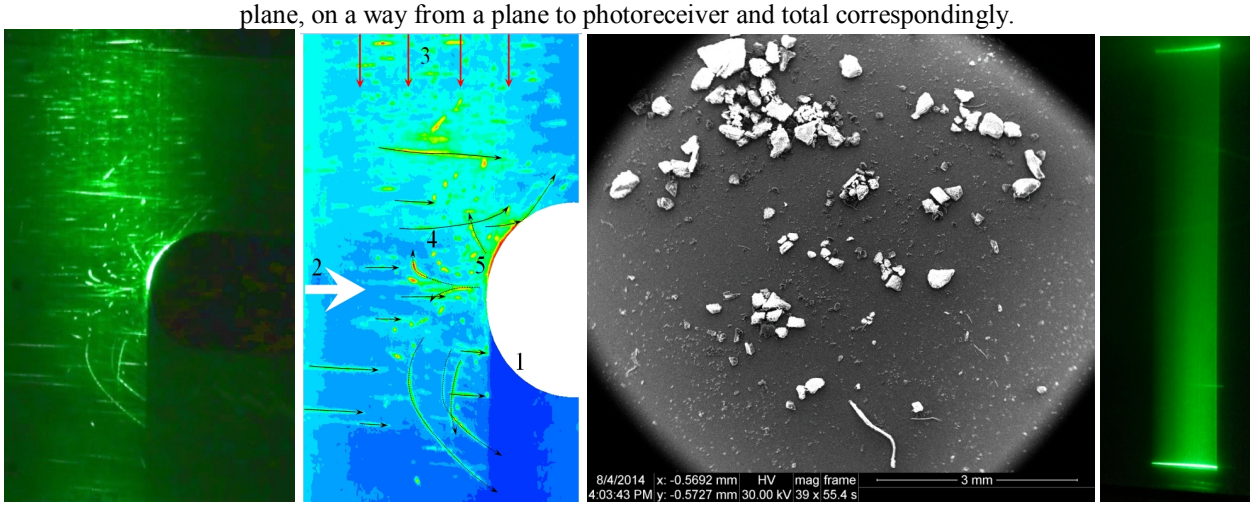

Fig. 8: Two phase flow optical investigation in icing wind tunnel and results of parallel laser sheet image analysis: 1 – aerosol flow direction, 2 – circumfluent body (wing profile), 3 – light direction in a laser sheet plane, 4 – tracks of rebounded particles, 5 – region of high concentration of particles. On the right: nonspherical electron microscope image, laser sheet geometry image.

Measuring scattered light intensity at different angles one can obtain a system of nonlinear algebraic equations in order to determine particles' size distribution and mass concentration of fractions in a 2D laser sheet plane.

Taking into account Bouger's light extinction photo receiver will register the following light intensity:

$$I_{\mathrm{F}}(y,\theta) = I(y,\theta)\cdot\cos\varepsilon\cdot\exp\left[-\frac{3}{4\rho_p}\int_0^S\left(\sum_{i=1}^{i_{\max}}\frac{\rho_i(s)}{a_p^i}Q_\lambda^{\mathrm{Ext}}(a_p^i)\right)\mathrm{d}s\right],$$

where s – way from a point of laser sheet plane to the photo receiver. The calibration of optical system is based on comparison of laser sheet image brightness and weight measuring of particles' concentration.

5 Supercooded water crystallization in aircraft icing process

Supercoolled water droplet crystallization after impingement and its adhesion (to an aircraft surface) mechanisms are fundamental problems in mechanics of the multiphase flows as well as in a condensed-matter physics. A physical model of the crystallization beginning in a supercooled droplet is proposed in present work. A minimal impingement impingement velocity of a droplet which is necessary for

crystallization is given by the following expression: $V_* = \sqrt{\frac{2w_c(T)}{\rho_l}}\exp\left[-\frac{\rho_l V_*^2 a_d}{6\sigma_l}\right]$.

Here a_d is a droplet radius, ρ_l and σ_l – droplet's liquid density and surface tension coefficient correspondently. $w_c(T)$ – intermolecular interaction energy density, which depends on physic-chemical properties of molecules, their orientation in a space which is also depends on temperature. The last expression takes into account conditions under which supercooled droplets will not crystallize after impact on a surface. The expression could be applied in ice accretion simulation in the aerosol flow with supercooled droplets.

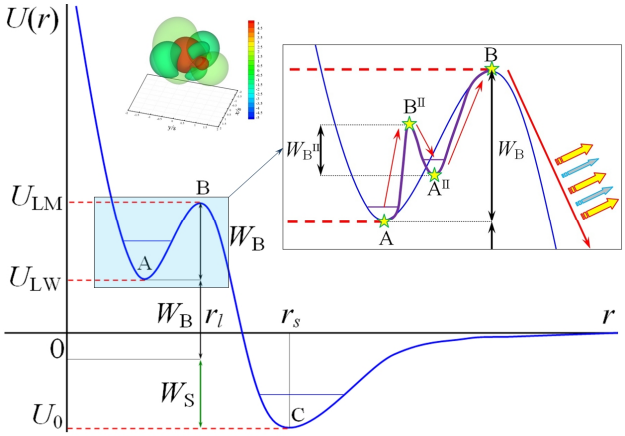

Fig. 9: Illustration of the mechanical energy accumulation effect in terms of multiholes water intermolecular interaction potential wells. After overcomming potential barriers a fraction of intermolecular energy transforms into electromagnetical energy.

In present work experiments were carried out and showed that an appearance of supercooled water crystallization could be not only due to significant mechanical pulse but also by several smaller ones. The effect of accumulation of mechanical energy could be explained as a presence of several potential wells in intermolecular interaction potential (Fig. 9). After mechanical impact a molecular system organization changes. It corresponds to another potential well. Thus potential barriers could be overcome via several mechanical impulses. In present work an equation liquid process is proposed in order to take into account ice crystals mass fraction α, front crystallization velocity V_{fC}, supercooled liquid temperature T_l and a temperature of liquid-ice mixture T_{ls}: $\chi_{sl}(\Delta T) + \lambda_l\left[\frac{\partial T_l}{\partial n} - \left(1-\alpha\frac{\rho_l}{\rho_s}\right)^{-4}\frac{\partial T_{ls}}{\partial n}\right] = L_{ls}\rho_l\alpha V_{fC}$.

Here L_{ls} – ice specific heat of fusion, λ_l – heat conduction of a liquid coefficient, χ – is an energy per unit of square and time which is due to infrared phase transition radiation, n – is a normal to the скныефддшяфешщт front. Mass fraction of ice crystals α which form after crystallization front motion depend on temperature according to the following expression $\alpha(\Delta T) = \sqrt{\Delta T / T_c}$, where temperature T_c = 156 K obtained from experiments. On the basis of experiments and described above model a fraction of additional energy could be estimated as follows: $\chi_{sl}(\Delta T) \approx L_{ls}\rho_l\alpha V_{fC}(\Delta T) - \lambda_l[(1+\alpha(\rho_l/\rho_s))^4 - 1]\frac{\Delta T}{\delta}$

Here δ – is a characteristic size of the interphase boundary between two phase mixture and liquid apart crystallization front.

6 Mathematical simulation of nonspherical particles' motion

As a characteristic size of a particle or droplet becomes smaller an influence of their Brownian motion becomes significant as well as their sensitivity to turbulent pulsations of the carrying gas. These effects can lead to the stochastic character of particles' or droplets' motion which significantly affects their interaction with circumfluent body. Randomness of particles' motion could be also due to their non-spherical shape, which leads to appearance of additional aerodynamic forces and torques. Mathematical simulation of nonspherical particles motion in gradient flows is an actual fundamental problem in multiphase flow physics. Nonspherical shape of particles leads to a variety of their trajectories and evolution of their concentration n_p near a circumfluent body: $\partial n_p / \partial t = S_{NS}\Delta n_p$ In present paper an expression of nonspherical crystals' scattering

coefficient S_{NS} for low Reynolds numbers of particles' motion in a reference frame which is connected with flow: $S_{NS} = (4\rho_p^2 a_p^4 / 81\mu^2)\beta^2(1-4\beta)(\boldsymbol{V} - \boldsymbol{V}_p)^2$. Here β is a coefficient which defines the difference between Stokes drag coefficient of spherical and nonspherical particles. Other quantities were described above.

7 Conclusions:

In application to based on particles flow investigations methods a correction method was developed in order to take into account a difference between particles' velocity and gas velocity. A criterion of two-phase flow nonequilibrium velocity fields' determination is proposed. Pressure, temperature and density fields' determination algorithms via particles' velocity fields' processing were developed. Results of images processing were obtained. A panoramic method of particles size distribution of a polydisperse flow in a laser sheet plane is propose. Original methods of two-phase flow parameters determination via inverse problems (of flow parameters determination via optical measuring) solution were developed in order to increase information from the laser sheet image. Mathematical models of physical phenomena which take place in the icing process were developed.

Acknowledgements

The work is supported by Russian fond of fundamental research No 13-01-00766, and also as a part of project HAIC (High Altitude Ice Crystals) of the 7-th European frame program as well as NIR "Basa".

References

[1] Vasilevskii E.B., Osiptsov A.N. (1999) Experimental and numerical study of heat transfer on a blunt body in dusty hypersonic flow. *AIAA Paper* N99-3563, pp 1–11.

[2] Tedeschi G., Gouin H., Elena M. (1999) Motion of tracer particles in supersonic flows. *Exp. Fluids*, vol. 26, pp 288–296.

[3] Miller A.B., Potapov Yu.F., Stasenko A.L. (2014) Experimental and theoretical investigation of aircraft icing in the case of crystal and mixed-phase flow. In: Proceeding of the 29th Congress of the International Council of the aeronautical sciences. – September 7th–12th. – 2014, Paper No 0576.

[4] Ragni A., Esposito B., Marrazzo M. Bellucci M., Vecchione L. (2005) Calibration of the CIRA IWT in the high speed configuration. In: Proceeding of the 43rd AIAA Aerospace Sciences Meeting and Exhibit. – Reno. – Nevada. AIAA 2005–471.

[5] J. Findeisen, M. Gnirß, N. Damaschke, H.P. Schiffer, C. Tropea (2005) 2D – Concentration Measurements Based on Mie Scattering using a Commercial PIV system. In: Proceeding of the 6th International Symposium on Particle Image Velocimetry Pasadena. – California. – USA. – September 21th –23th. – 2005. – PIV'05.

[6] Ghaemi S., Ragni D., Scarano F. (2012) PIV-based pressure fluctuations in the turbulent boundary layer. *Exp. Fluids*, vol. 53, pp 1823–1840.

[7] Koike S., Tamura T., Masua G. (2009) Influence of Drag Coefficients and Velocity Fluctuation on PIV Correction Method. *AIAA J.*, Copyright AIAA PIV 47th AIAA Aerospace Sciences Meeting. – Orlando. – Florida, pp 1–17.

[8] Henderson C.B. (2009) Drag coefficients of spheres in continuum and rarefied flows. *AIAA J.*, vol. 14, No 6, pp 707–708.

[9] Dring R.P. (1982) Sizing criteria for laser anemometry particles. *J. Fluids Eng.*, vol. 104, pp 15–17.

[10] Melling A. (1997) Tracer particles and seeding for particle image velocimetry. *Meas. Sci. Technol.*, vol. 8, pp 1406–1416.

[11] Amelyushkin I.A. (2014) Way of particle numeric concentration field measurement in the aerosol flow and the way of its realization. *Patent* No №2014119714 from 16.05.2014 (in Russian).